The Aquifer-CO2Leak project: Numerical modeling for the design of a CO2 injection experiment in the saturated zone of the Saint-Emilion (France) site

Omar Gassara, Audrey Estublier, Bruno Garcia, Sonia Noirez, Adrian Cerepi, Corinne Loisy, Olivier Le Roux, Anelia Petit, Lena Rossi, Sean Kennedy, et al.

The Aquifer-CO_2Leak project: numerical modeling for the design of a CO_2 injection experiment in the saturated zone of the Saint-Emilion (France) site

O. Gassara[a], A. Estublier[a,*], B. Garcia[a], S. Noirez[a], A. Cerepi[b], C. Loisy[b], O. Le Roux[b], A. Petit[b], L. Rossi[b], S. Kennedy[b], T. Brichart[c], P. Chiquet[d], L. Luu Van Lang[d], F. André Duboin[e], J. Gance[f], B. Texier[f], B. Lavielle[g], B. Thomas[g]

[a]*IFP Energies nouvelles, 1 et 4 avenue de Bois-Préau, 92852 Rueil-Malmaison Cedex, France*
[b]*EA 4592 G&E ENSEGID-Bordeaux-INP, 1 allée F. Daguin, 33607 Pessac cedex, France*
[c]*Glincs S.A.S, 43 boulevard du 11 Novembre 1918, 69100 Villeurbanne, France*
[d]*Teréga, 40 Avenue de l'Europe, 64000 Pau, France*
[e]*International Petroleum Corp., 51210 Montmirail, France*
[f]*IRIS Instruments, 1 Avenue Buffon, 45100 Orléans, France*
[g]*CENBG, 19 Rue du Solarium, 33170 Gradignan, France*

Abstract

The objective of the Aquifer-CO_2Leak project is to get insights into carbon dioxide CO_2 migration in aquifers within the context of Carbon Capture and Storage (CCS) and to test the different equipment necessary for CO_2 monitoring. The underlying idea is to develop an experiment in the saturated zone (phreatic) of the underground limestone quarry located at Gironde department (France). It consists in injecting water, carrying dissolved gases (CO_2 and krypton) and a fluorescent molecule, under controlled conditions. In this paper, we present the dimensioning study of the experiment by numerical simulations carried out using the simulator CooresFlow (IFPEN's in-house simulator for reactive transport in porous media). The important experiment parameters (injection flow rate, injected volume, the time to return in system equilibrium and wells location) were successfully estimated. In particular, the variation of species concentration in time and space was simulated and analyzed to define an experimental measurement schedule for the planned survey. Finally, a sensitivity analysis of the uncertain model parameters is presented. We found that the water table level and the dispersivity of the

*Corresponding author
Email address: audrey.estublier@ifpen.fr (A. Estublier)

porous medium appear to be the most "sensitive" parameters.

Keywords: CO_2, carbon capture and storage (CCS), saturated zone, porous media, experimental site, near-surface hydro-geological and hydro-geochemical.

---

1. Introduction

The average global temperature on Earth has increased by 0.9° Celsius since the beginning of the industrial era [1, 2]. In particular, two-thirds of the warming has occurred at a roughly rate of 0.15-0.20°C per decade since 1975. The phenomenon of global warming that is basically induced by the rise in global temperature has been the origin of numerous destructive effects on the planet: sea level has risen by 10 to 20 centimeters in certain area, the distribution of precipitation shifted throughout the 20th century, and extreme climate phenomena such as tsunamis or tropical storms became evermore frequent. The main contributor to these detrimental effects was identified as one of the main greenhouse gases, which is Carbon dioxide (CO_2). Indeed, in 2013, the atmospheric concentration of CO_2 exceed 400 parts per million (ppm) for the first time in recorded history [3]. Plants of power, cement, steel or incineration are the main causes for this recent relentless rise in CO_2 concentrations in the atmosphere. However, these industries do not currently have alternative technologies to massively reduce their CO_2 emissions.

Carbon Capture and Storage (CCS) is an auspicious measure for reducing or preventing CO_2 from reaching the atmosphere. The idea consists in separating CO_2 from the emissions of stationary point sources such as power plants or factories and pumping the purified and concentrated fluid into suitable storage sites in the subsurface [4, 5, 6, 7, 8]. We talk about geological storage as CO_2 is trapped in reservoir rocks under the ground. The storage areas can be of different nature: deep saline aquifers, depleted petroleum fields or coal seams. Deep saline aquifers appear to be the storage reservoir with the highest capacity utilization (400 to 10,000 CO_2 Gton) [9]. Nevertheless, their structure and potential to permanently trap CO_2 remains very hard to assess; therefore a significant research effort must be undertaken to bring answers on their long-term potential for the prospects of CCS.

One of the main features of an aquifer site for CO_2 storage is to present a minimal probability of leakage (no natural fracturing, sealing properties of the caprock, well in good condition, etc.) [10]. It has been proposed that a rate of 0.01 % per year of CO_2 leakage would be considered as the maximum tolerated risk for a CO_2 sequestration site [11]. Therefore, it is necessary to set up monitoring systems for CO_2 monitoring in order to detect these possible leaks, to assess their magnitude and their impacts and to predict possible corrective actions. Among the different monitoring techniques, the geochemical analysis that is the subject of this article, allows to monitor over time the fluids composition at soil surface and in wells [12, 13, 14, 15, 16, 17].

Monitoring CO_2 soil gas has been intensively studied in recent years (e.g. [13], [18]). For example, Myers et al. [19] used gas tracers in particular as precursors of CO_2 leakage to identify the origin of the CO_2 detected. There are few studies on the interaction occurring between the geological storage formation and the gas phase. In their study [20], Oldenburg and Unger explained that depending on the type of release, the attenuation efficiency of the unsaturated zone could be drastically different. The evaluation of the natural flux and soil gas baseline concentration is of primary importance when studying the influence of natural processes on soil gas dynamics. Indeed, natural biological activity can induce variations of several percent in volume content of CO_2 in soil atmosphere ([21], [16], [22]). The biological production of CO_2 is due to the organic matter degradation or roots respiration ([22]). Monitoring techniques for soil gas composition study have been extensively developed as a part of environmental and ecological applications. Different protocols for monitoring gas composition in soil have been developed for application as a routine tool ([20], [22]). Due to the natural fluctuation of biological activity induced by seasonal variation, the period of investigation to determine the baseline soil gas composition is of primary importance. For example Gal et al. [13] proposed a period of 18 months of monitoring for baseline evaluation as a reasonable timescale to evaluate the global natural cycle of CO_2 in soil. A baseline soil gas monitoring along several years could be required as well, since seasonal variation could differ year after year, especially in a context of climate change. In the experiment at the ZERT controlled release site, Cranfield experimental site, CO_2 gas was injected in shallow water and the released CO_2 was monitored at the

soil surface with repeated grid measurements of soil CO_2 gas fluxes [21]. The authors concluded in their article to careful characterize the background CO_2 variability prior to CO_2 injection into the storage reservoir, to limit the total area of investigation by focus on features most susceptible to leakage (e.g., wells, faults) and to use various complementary CO_2 measurement techniques in a program of storage site monitoring.

Similarly, water-mineral chemical reactions can be a source or a sink of CO_2. The carbon dioxide concentration is also particularly affected by soil temperature due to the strong dependence between temperature and chemical/biological reaction rates ([23], [16], [22]). Concerning the liquid phase and the interface between the liquid phase and the gas phase (in the capillary zone in a natural context at subsurface location, between the saturated and the non-saturated zones), several techniques have also been developed (examples of sampling tubes, in-situ probes) but only few studies have put in evidence the influence of natural parameters variations (porosity, permeability, level of water table) on the CO_2 migration, its detection, and the degassing phenomenon that can occur.

Herein, this Aquifer-CO_2Leak project is part of this research work necessary for the monitoring, the verification-characterization, and the geochemical detection of CO_2 leaks as well as the prediction of CO_2 behavior from reliable numerical models in near-surface environments, more particularly, in the saturated zone. It consists in experimenting CO_2 injection in not deep aquifer (phreatic) at Saint-Emilion in France on a site already well characterized from the hydrogeological and geochemical point of view. The aim is to get better understanding of CO_2 behavior in the saturated zone, to develop a know-how on the different aspects related to a CCS project (such as site characterization, injectivity control and leakage detection), and to test various geochemical and geophysical monitoring equipment and methods. In this article, we focus on the geochemical approach of this project that tests noble gases and a fluorescent molecule as tracers in the aquifer.

The main objective of this paper is to present the predictive modeling results of this small pilot-scale CO_2 injection experiment. The simulations have been carried out to design the pilot with the following purposes: (1) determining the volume of injected water enriched with dissolved CO2 and tracers, the injection rate and the amount of

CO_2 and tracers to be injected in the saturated zone in such a way that their migrations can be followed with a sufficient precision, (2) predicting the carbonated water plume and the total time to return to the initial state of the domain, (3) determining the optimal location of the different geochemical sensors well for sufficient measurement coverage, and (4) defining as precise as possible a schedule for the measurements and/or sampling.

2. Site description and selection of the zone of interest

2.1. Saint-Emilion experimental site

The experimental site is an abandoned underground limestone in Saint-Emilion, in Nouvelle Aquitaine (France), exploited by "the rooms and pillars" method. It consists in an immense 70-hectare network of underground galleries that form a gigantic network of paths and developed on 3 levels. The carbonate formation is dated at Upper Oligocene (Stampien, 28-30 Ma) in Nouvelle Aquitaine basin and is composed of wackestone to grainstone facies characterizing an inner intertidal ramp platform. These carbonate facies are affected by a deep meteoric diagenesis process during 28-30 Ma. This geological emmersif event develops a good secondary porous network and a good porosity and permeability in the studied carbonate formation. The map of this underground quarry is shown in Figure 1 (a). The black lines represent the limits of each underground rooms or gallery. Pillars in gray are displayed on the map. The unsaturated zone, of about 18 m in depth, overlies the water table. The level of the water table Z_{wt} is given by discontinuous blue lines and expressed in reference to the General Levelling of France (NGF). P5 and P6 denote respectively the reference well and the control well initially drilled in the site. The areas where drilling is possible (the height of the cavity is greater than 2 m) are marked in green and the areas where drilling is very complicated (the height is less than 2 m) in yellow. The underground water comes mainly from surface water infiltration due to effective precipitation. Some piezometric measurements were made near the reference well P5 that allowed us to determine the seasonal changes in the water table level and to estimate the hydraulic gradient at this area of the experimental site. More details about the geological properties can

be found in Loisy et al. (2013) [16] and Garcia et al. (2013) [17]. All the gathered measurements are reported in Figure 1 (b) that depicts a cross-section of the part between the substratum and the gallery floor along the discontinuous black line shown in Figure 1 (a).

The domain is composed of 4 layered parts: (1) a layer of thickness that varies between 0 and 0.5 m of backfill; this backfill was added in order to ensure a flat gallery floor, (2) a first layer of limestone with a maximum thickness of 1 m; the porosity in this layer varies between 0.35 and 0.45 and the permeability ranges from 10 to 14 D, (3) a second layer of limestone with a thickness of 3.5 m; the porosity is between 0.2 and 0.35 and the permeability varies from 6 to 10 D, and finally (4) an impermeable and nearly flat layer of clay named the sannoisian green marls; this layer is located at a total depth of 19.4 m (the soil altitude is 79.9 m NGF). Two extreme water table levels were measured depending on the hydrogeological recharge, a highest (January to February) and a lowest (June to July) water table. The maximum oscillation of the water table (zone of intermittent saturation) is 1.5 m. Furthermore, the measured hydraulic gradient i is of 5 % regardless the water table level.

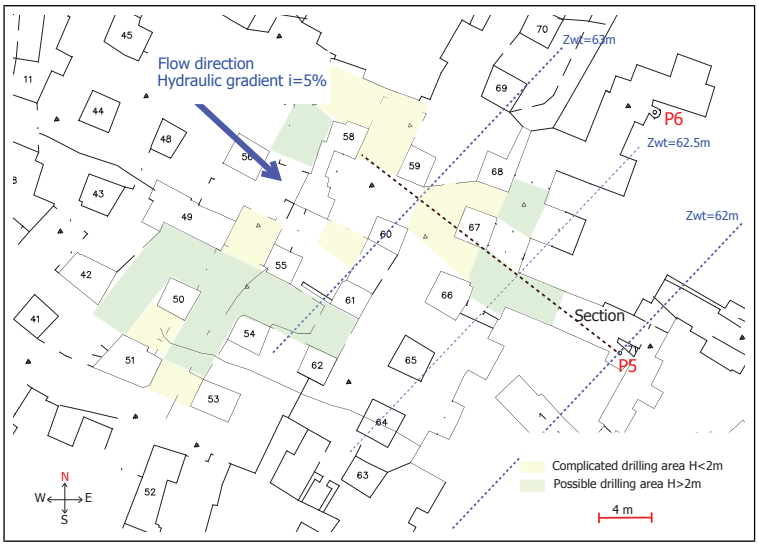

(a)

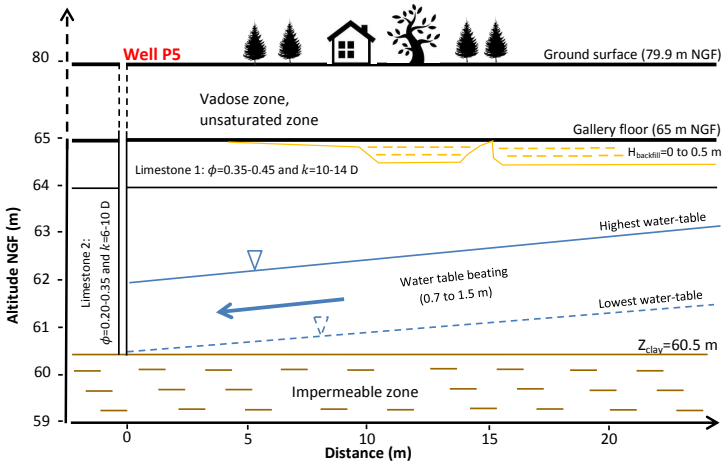

(b)

Figure 1: (a) Map of Saint-Emilion site (underground view): the numbered pillars in gray are displayed on the map. Three different water table level ($Z_{wt} = 62$, 62.5 and 63 m) were measured and shown in the figure by discontinuous blue lines leading to an hydraulic gradient i equal to 5 %. The flow direction is from the top left to the bottom right as given by the big blue arrow. P5 and P6 denote respectively the reference well and the control well initially drilled in the site. The areas where drilling is possible (the height of the cavity is greater than 2 m) are marked in green and the areas where drilling is very complicated (the height is less than 2 m) in yellow; (b) Conceptual scheme of the aquifer near the reference well P5 and along the discontinuous black line shown in (a).

2.2. Zone of interest

In order to define our simulation model, we have chosen a zone of interest on the site. The underlying idea is to cover the maximum of the green zone where the drilling is possible for both injection and observation. The selected zone is shown in red square in Figure 2 (a). Note that the dimensions of the domain are 20 m $\times$ 20 m and the model axes are oriented with the zone geometry. The Y-axis is parallel to the water flow direction in the aquifer (according to the hydraulic gradient), the X-axis is perpendicular to it and the Z-axis is set at the gallery surface. Furthermore, in order to estimate the water table level in this area, we extrapolated the measured hydraulic gradient ($i = 5$ %) to this zone and we kept the same flow direction in all areas. As shown in Figure 2 (a), the injection well is centered on the transverse (with respect to the flow direction) X-axis, that is its coordinates are ($X = 10$ m, $Y = 14.8$ m). Two observation wells are positioned parallel to the Y-axis and aligned with the injection well: the first one is at a distance of 3 m and the second at 6 m from the injection. A third observation well is placed at the following coordinates ($X = 14$ m, $Y = 4.8$ m), that is an offset of 4 m with respect to the flow direction.

In order to get a clear idea about the studied zone disposition, we present in Figure 2 (b) a conceptual scheme of the underground at the YZ section. The aquifer shape was depicted by a top-angled trapezoid model geometry where the bottom is horizontal, and the left and the right corner are vertical. The dip angle of the aquifer top represents the hydraulic gradient i which was set at 5 %. Following this representation, the water table level Z_{wt} in the domain varies between 62.75 and 63.75 m (NGF) leading to a maximum depth of 2.25 m with reference to the gallery floor. Note that the highest water table was chosen to depict the aquifer top. The model include an ambient formation water flow from the higher situated east boundary to the lower west boundary. Furthermore, the aquifer petro-physical properties are represented by the second layer of limestone (cf. Figure 1 (b)).

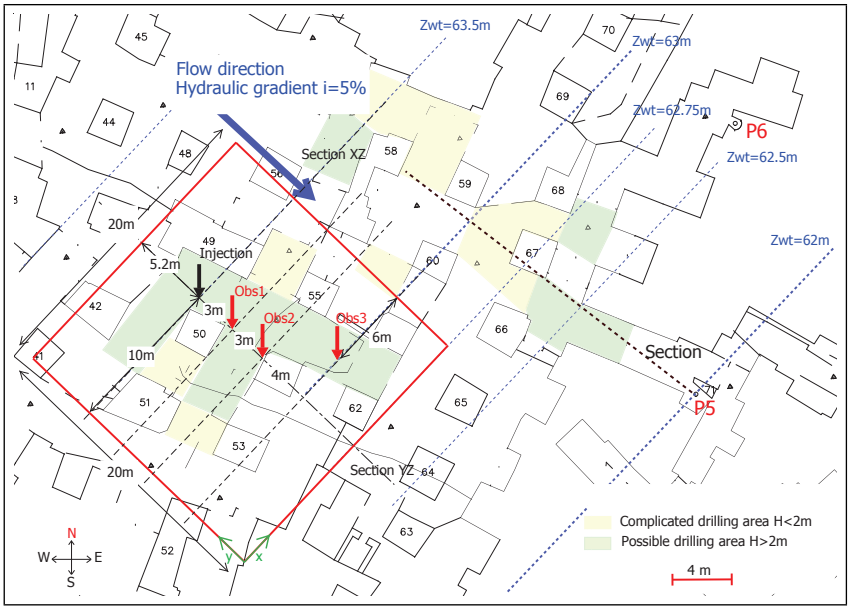

(a)

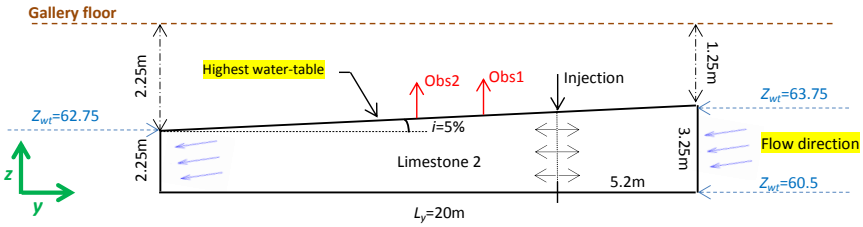

(b)

Figure 2: Selection of the Zone of interest: (a) placement and dimensions of the selected zone on the experimental site of Saint-Emilion. The selected zone is shown in red square which covers the maximum of the green areas that offer an easier drilling for injection and observation. The position of the injection well is pointed by a black arrow and the three observation wells by red ones (Obs1, Obs2 and Obs3); (b) conceptual scheme of the YZ section of the selected zone that depicts the aquifer shape.

3. CooresFlow Software and modeling framework

3.1. General characteristics

In our publication, the numerical simulations allowing to realize the design of the pilot were carried out with CooresFlow ([24], [25], [26]), IFPEN's in-house research simulator for reactive transport in porous media. It is developed in parternship with international industries and academics to model multiphase transport processes coupled with fluid-rock interactions, for various applications including CO_2 underground storage as well as enhanced recovery of hydrocarbon reservoirs.

CooresFlow is a THC (thermal hydro-chemistry) simulator that considers the following phenomena: (a) multiphase flow in porous media, with viscous and capillary forces, (b) transport of chemical components by advection, diffusion and dispersion, (c) transfers within the fluids or on the surface of the rock governed by local equilibrium, (d) chemical equilibrium or kinetic reactions to describe geochemical exchanges, (e) heat convection and thermal conduction, and (f) dynamic modification of the porosity and permeability of the porous medium over time.

Numerous numerical simulators model non-isothermal multiphase multicomponent transport processes with or without fluid rock interaction ([27], [28]). Amoung them, CooresFlow aims to be a useful tool either for understanding complex processes occuring in porous media and for modeling them, or for simulating the fluid flow, the species migration and the rock reactivity for real sites with a geological model integrating both the structural complexity and numerous lithologies. Thus, it proposes particular functionalities: (1) modular physical models such as generic (e.g. EOS of Peng-Robinson) or user-defined (e.g. a new mathematical formula modeling a particular thermodynamical behavior) models, (2) unstructured meshes, (3) a friendly interface and (4) different complexity levels of coupling between the fluid flow model and the geochemical model associated to a parallel computing.

3.2. Mathematical formulation of a compositional monothermal single-phase flow model

The study concerns the simulation of water injection containing the following dissolved species (CO_2, krypton and fluorescent molecule) in the saturated zone. To carry

out this study, we used the following physical model: a compositional single-phase flow model that accounts for advection, dispersion and molecular diffusion within non-thermal context. It is worth noting that in this work, we will not consider the coupling between flow and reactive transport mechanisms. Indeed, the chemical reactions that may occur between solid and liquid have been neglected in a first time for the sake of simplicity. However, the rock-fluids interaction will be considered in the future works of this project and the effect of mineral dissolution and precipitation on a long term CO_2 migration will be studied and analyzed.

The compositional flow model used in this study is based on the following material balance equations:

$$\frac{\partial C_j^\alpha}{\partial t} + \mathrm{div}(J_j^\alpha) + Q_j^\alpha = 0 \tag{1}$$

where α is the water phase, j the species index, C_j^α the molar concentration of the species j [mol.m^{-3}], J_j^α the vector of molar flow rate of species j [mol.s^{-1}.m^{-2}], Q_j^α the source term (well) [mol.s^{-1}.m^{-3}].

In addition, the following laws are used to describe fluid flows and transfers in the porous medium:

Generalized Darcy's law for fluid flow:

$$V^\alpha = -\frac{K}{\mu^\alpha}\left(\nabla P^\alpha - \rho^\alpha g\right) \tag{2}$$

Species transport by advection:

$$J^\alpha_{j,\,\mathrm{adv}} = C_j^\alpha V^\alpha \tag{3}$$

Fick's law [29] for species diffusion/dispersion of species:

$$J^\alpha_{j,\,\mathrm{Diff}} = -\left(D_j^\alpha + \mathrm{Disp}^\alpha\right)\cdot\nabla C_j^\alpha \tag{4}$$

Where P^α is the pressure of the phase α [Pa], V^α is the velocity of the α phase [m.s^{-1}], K is the medium permeability [m^2], μ^α is the viscosity of the α phase [Pa.s], ρ^α is the density of the α phase [kg.m^{-3}], g is the gravity constant [m.s^{-2}], D_j^α is the diffusion tensor of a species j in the α phase [m^2.s^{-1}], Disp$^\alpha$ is the dispersion tensor in the α phase [m^2.s^{-1}] characterized by α_L the longitudinal dispersivity coefficient [m] and α_T the transversal dispersivity coefficient [m].

4. Physical and numerical model

Figure 2 (b) shows the setup that was chosen for the three-dimensional simulation model. The simulation geometry was finely-meshed along the three axes X-Y-Z with constant space steps discretization: $\Delta X = 20$ cm, $\Delta Y = 20$ cm and $\Delta Z = 16$ cm, leading to $100 \times 100 \times 20$ cells. The cells size was carefully chosen to capture the physical phenomena detailed above as well as to limit the numerical dispersion. The domain is limited by boundary conditions: a hydrostatic pressure on both sides $y = 0$ and $y = 20$ m and a zero flux condition on the other faces, leading to an underground water velocity of 0.15 m/day (along the Y-axis). Concerning the initial conditions, the temperature T was set at 14 °C and the pressure P at the hydrostatic pressure as $P = 1$ bar at a depth of 1.25 m (at the higher situated east boundary), and the porous medium was supposed to be fully saturated with water carrying 15.5 mg/l of dissolved CO_2. In addition, the water density ρ_w and viscosity μ_w were assumed to be constant at 1000 kg/m^3 and 1 cP, respectively, whatever the water is carrying CO_2 and krypton or not. Indeed, the impact of water density and viscosity differences in presence of dissolved gases on the flow is expected to be negligible in the studied case since at 1 bar and 14 °C the density of water enriched with CO_2 reaches only 1001 kg/m^3 and the viscosity is close to 1 cP.

The petro-physical properties of the domain were fixed at the minimum values measured in the layer 2 of limestone (see section 2.1, [16]). The permeability k and the porosity ϕ were set constant as $k = 6$ D and $\phi = 0.2$ ([16]) because of lack of heterogeneity measurements in the zone of interest. Table 1 summarizes the physico-chemical properties of the different species dissolved in water that are considered in this simulation study. To complete the physical model, we have chosen at this stage of this study the following values for the field dispersivity by considering the scale 20m of the domain: the longitudinal dispersivity is as $\alpha_L = 1$ m and transverse dispersivity as $\alpha_T = 0.33$ m according to Gelhar et al. (1992) [30].

A 8 cm diameter well was placed as given by Figures 2. The injection rate was estimated assuming that the injection was over the entire column at a constant volumetric flow rate and the injection velocity was close to the initial water velocity in the water table such that we limit overpressure around the well. Thus, the calculated injection

Table 1: Physico-chemical properties of species dissolved in water at $T = 14°C$ and $P = 1$ bar.

	Molar mass ($g.mol^{-1}$)	Diffusion coefficient in Water ($cm^2.s^{-1}$)	Solubility in water (KI)
H_2O	18.01	2.30×10^{-5}	-
CO_2	44.01	1.41×10^{-5}	1,610
krypton	83.80	1.51×10^{-5}	17,700
fluorescent molecule	18.01	2.30×10^{-5}	-

rate is $Q_{\text{inj}} = 4.2 \times 10^{-5}$ m^3/s = 2,520 ml/min. The injected water volume was estimated taking into account the porous volume of the pilot and the difficult conditions for moving experimental materials. Thus a total injected volume of 200 l was considered that represents 0.1 % of the pore volume PV (PV = 220 m^3) as the porosity is equal to 0.2. It leads to an injection time of 78 min. After the injection stage, we close the well and we simulate the migration of the dissolved species over 20 days. The imposed molar fraction x_i and mass fraction w_i (ppm) of each species i dissolved in the injected water are as follows:

$$\begin{cases} x_{\text{H2O}} = 9.98 \times 10^{-1} \\ x_{\text{CO2}} = 6.21 \times 10^{-4} \\ x_{\text{kr}} = 5.65 \times 10^{-5} \\ x_{\text{fluo}} = 1 \times 10^{-3} \end{cases} \Longrightarrow \begin{cases} w_{\text{H2O}} = 997,220 \quad (\text{ppm}) \\ w_{\text{CO2}} = 1,515 \quad (\text{ppm}) \\ w_{\text{kr}} = 262 \quad (\text{ppm}) \\ w_{\text{fluo}} = 998 \quad (\text{ppm}) \end{cases}$$

On one hand, by following these imposed values, the CO_2 and the krypton were injected at the maximum dissolved amount under the fixed temperature and pressure conditions. On the other hand, the injected amount of the fluorescent molecule was set at an arbitrarily chosen low value.

5. Results and discussions

In this section, we present the obtained simulation results and the discussions needed, by following this sequencing: first, a physical description of species concentra-

tion dynamics in the cross-section YZ (Figure 2 (a)) is presented in both the injection and the post-injection stage. Then, we study the temporal evolution of the CO_2 mass fraction in the three observation wells and its plume at several time steps. Finally, we consider the concentration variation of the components across the XZ cross-section in order to better understand their migration and their spreading along the longitudinal and the transverse direction to the main water flow.

Figures 3 (a) and (b) show the dynamics of CO_2 mass fraction in the cross-section YZ of the injection well during both the injection and the post-injection stage. When the injection starts, the concentration of CO_2 increases by steps in the vicinity of the injection well until reaching a maximum value of $w_{CO2} = 1,100$ ppm after a total injection time of 78 min. The latter maximum value is a little smaller than the imposed one due to the dispersion phenomenon taken into account in this study. At the end of the injection stage, the injected CO_2 is present at a maximum distance of 1.5 m from the injection well and even behind it (at the opposite of main water flow direction) due to a low overpressure induced by injection, but it does not reach the observation wells. Once the injection is stopped, the CO_2 concentrations spread rapidly in the direction of flow as the simulated profiles show smooth transitions with a maximum value that does not exceed 40 ppm after 3 days. Indeed, as time increases, the concentration profile decays, advects in the aquifer flow direction with high velocity, and spreads outward. After 10 days, the injected CO_2 expands over the entire length of the section attesting for a great dispersion effect. This important concentration spreading is essentially due to dispersion, and more particularly to the longitudinal dispersivity, which remains the preponderant phenomenon in saturated ground-water flow as it dominates molecular diffusion.

We found that the same observations can be made for the krypton migration along the Y-Axis, as shown in Figures 3 (c) and (d). Similarly, the concentration of the krypton increases steeply during the injection stage to reach the maximum value $w_{kr} =$ 190 ppm, then it spreads rapidly and follows the same trend observed in CO_2 migration. The only differences that have been found concern the maximum concentration values. For both CO_2 and krypton, the maximum concentration corresponds to 73 % of the initial concentration that confirms the process of migration is mainly advection and

dispersion and not diffusion. This observation applies also to the fluorescent molecule transport. For this, in the following of this work, we focus our analysis on the migration of a single component, which is CO_2, since the same remarks remain valid for the various species.

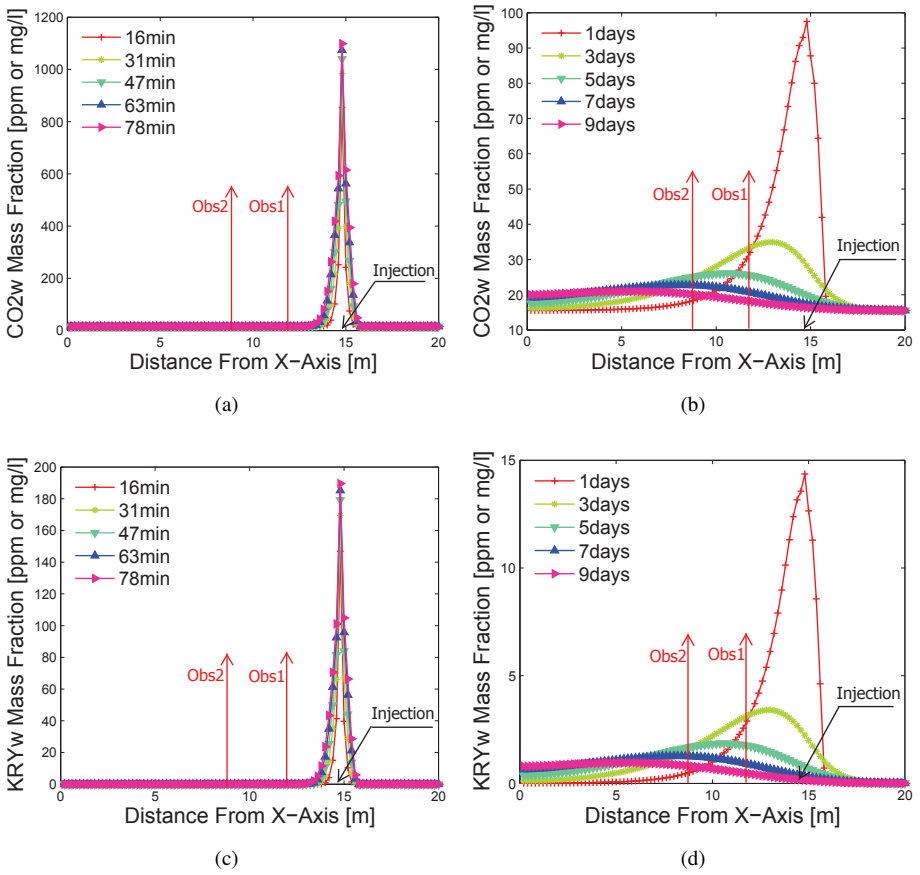

Figure 3: Dynamics of CO_2 and krypton mass fractions along the section YZ of the injection well, during: (a) and (c) the injection stage, (b) and (d) the post-injection stage.

We are interested now in studying the temporal evolution of CO_2 concentration in the three observation wells (Obs1, Obs2 and Obs3). The obtained results are shown in Figure 4. Few hours after the injection stop, the injected CO_2 breaks through the first observation well (Obs1), then increases in time until reaching a maximum value

of 37 ppm after 2 days, and finally, decreases rapidly to the initial value (15.5 ppm). Concerning the second observation well (Obs2), the maximum value of CO_2 mass fraction that can be measured is 26 ppm and it can be recorded after 4 days. Located at 10 m from the injection point and at 4 m from the CO_2 plume center, the (Obs3) well is reached by CO_2 due to the transversal dispersion. The maximum value is 17 ppm at 9 days which is close to the initial value (15.5 ppm). The Figure 4 also shows that the system returns at its initial state after 20 days.

To get an idea about the dissolved CO_2 migration and plume temporal evolution, we present in Figures 5 (a), (b) and (c) screenshots that show a top view of the CO_2 concentration distribution at times when the maximum of CO_2 is reached at each observation well during the post-injection stage. The effect of the longitudinal and transverse dispersivity is clear on CO_2 migration. At 2 days, the plume is of approximately elliptic shape with dimensions as follows: $L_L = 3$ m and $L_T = 1$ m, where L_L denotes the longitudinal (main axis) spreading and L_T the transverse (minor axis) one. After 4 days and when it reaches the second well, the CO_2 concentration spreads and the plume gains enormously in size as its dimensions become $L_L = 6$ m and $L_T = 2$ m. Finally, after 8 days from the injection, the CO_2 plume advances mainly along the Y-axis and covers a huge part of the domain ($L_L = 12$ m and $L_T = 4$ m) but with very low concentrations. Thus, the dissolved CO_2 plume just reaches the third observation well (Obs3) because it is located at 4 m from the plume center. It reaches the model boundary already after less than 10 days.

To get more clarity about CO_2 migration, we study the dynamics of CO_2 mass fraction in the three cross-sections XZ of the observation wells. The corresponding results are reported in Figure 6. The maximum values that can be measured in each well and the plume extensions are still clear in this figure. Still some additional remarks can be made according to the CO_2 distribution. We found that the simulated profiles show a spreading Gaussian cloud which is centered on the main water flow direction and advances due to advection and dispersion as noted before. Indeed, as a function of time, the maximum value decreases between the three sections while the width of the spreading increases significantly. Note that the maximum value shown in Figure 6 (c) is 22 ppm which is different to the one recorded in Obs3 as the latter well is located at

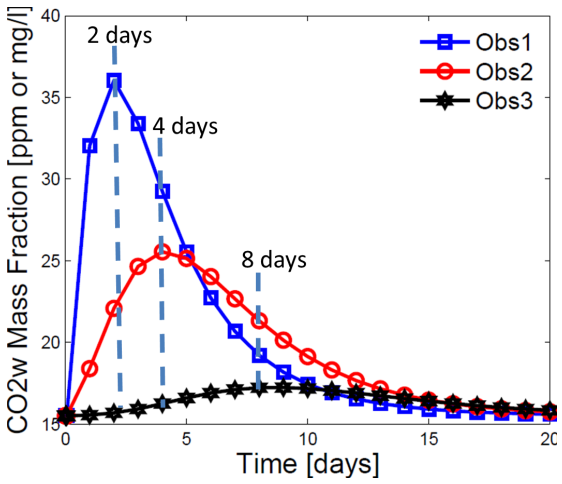

(a)

Figure 4: Evolution of the CO_2 mass fraction in water versus time (in the observation wells).

$X = 14$ m, that is an offset of 4 m from the main plume axis.

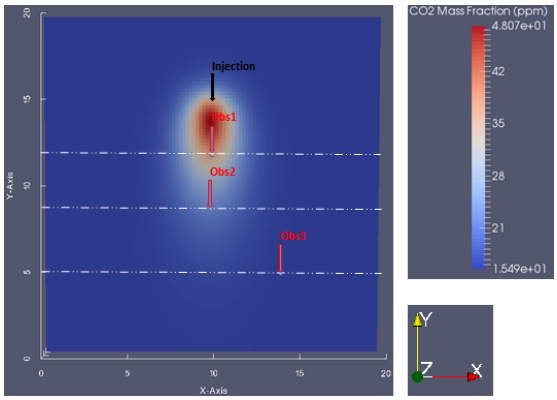

(a)

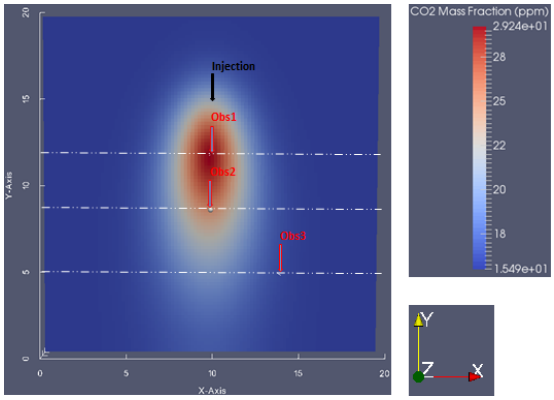

(b)

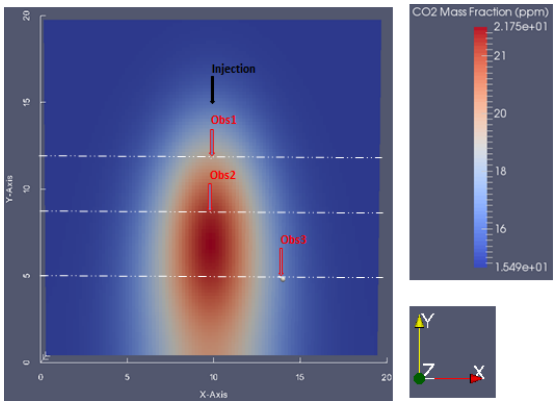

(c)

Figure 5: Zoom-in at the top view of the dissolved CO_2 plume at times when the maximum of CO_2 concentration is reached at each observation well during the post-injection stage: (a) after 2 days, (b) after 4 days and (c) after 8 days. The scales are adapted by figure.

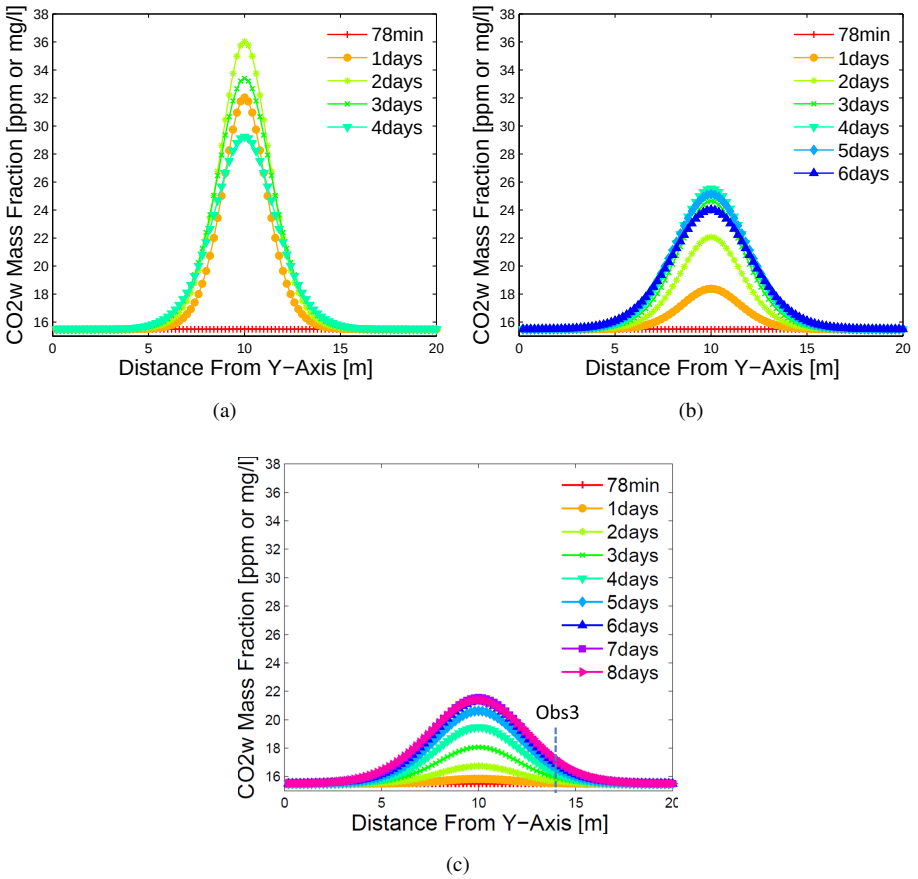

Figure 6: Dynamics of CO_2 mass fraction in the three cross-sections XZ of the observation wells: (a) Obs1 at 3 m, (b) Obs2 at 6 m and (c) Obs3 at 10 m from the injection well. Note that Obs3 is located at $X = 14$ m in figure (c), i.e. 4 m from the CO_2 plume center

6. Sensitivity study

The objective in this section is to provide information on the uncertainty associated with model simulations and to identify the most important parameters that have a strong influence on the model outputs. We begin this section by a discussion and a selection of the uncertain parameters in our study case which are due to lack of knowledge or even of measurements. Then, we focus on the one hand on the effect of the aquifer characteristics, which are the dip angle of the aquifer top-surface linked to the water table level, and on the other hand, on the effect of the petro-physical properties of the porous media (permeability, porosity, and dispersivity) on the CO_2 flow migration. In particular, the sensitivity results in terms of species concentration variations in space and time are presented and discussed in each simulation case.

6.1. Selection of the uncertain parameters

Until now, several parameters were estimated based on data gathered from surveys conducted on the site next to the zone of interest and from the literature or even by interpolating the available data. Indeed, in the primary model presented above, the permeability k and the porosity ϕ were fixed at 6 D and 0.2, respectively. In addition, we considered that the level of the water table is the highest measured one because we have scheduled to inject CO_2 in the aquifer in summer, period of high water table. The longitudinal dispersivity ($\alpha_L = 1$ m) and the ratio $\alpha_L/\alpha_T = 3$, where α_T denotes the transverse dispersivity, were also estimated from the literature [30]. Finally, we note that we considered a dip angle of 5 % along the Y-axis and none along the X-axis (no available data and not expected to be high) in our model which remains a strong assumption that we must verify during the scheduled CO_2 injection. For the sake of clarity, we will refer to this case as the "reference" case.

Accordingly, we chose to conduct our sensitivity analysis by performing the following simulations by:

- adding a dip angle of 1 % along the X-axis, such that the groundwater flow will be changed and becomes two-directional flow,

- considering the lowest level (in winter) of the water table Z_{wt}: Z_{wt} varies between 61.25 and 62.25 m (NGF) leading to a maximum depth of 3.75 m with reference to the gallery floor,
- using the maximum measured values of the permeability and the porosity in layer 2 of limestone (that is $k = 10$ D and $\phi = 0.35$),
- considering the two limit values (maximum and minimum) of the longitudinal dispersivity found in the literature for the scale of our model [30]: $\alpha_L = 0.33$ m ($\Rightarrow \alpha_T = 0.11$ m) and $\alpha_L = 3$ m ($\Rightarrow \alpha_T = 1$ m).

Note that we chose these extreme values in order to figure out the possible variation range of the model outputs. In the following, single parameters were varied while the others of the "reference" case were kept constant in order to emphasize the effect of each parameter. Table 2 summarizes all the parameters values used in this sensitivity study.

Table 2: Parameters values selected for the sensitivity study. The reference values are marked with the special character †. Note that the Y-axis is parallel to the main water flow direction in the aquifer (according to the hydraulic gradient), the X-axis is perpendicular to it.

Properties	Uncertain parameters	Measured-estimated values		
Aquifer	Dip angle	Y-5%†	Y-5% and X-1%	
	Level of water table Z_{wt}	Highest†	Lowest	
Petro-physical	Permeability, k (D)	6†	10	
	Porosity, ϕ (-)	0.2†	0.35	
	Longitudinal dispersivity, α_L (m)	0.33	1†	3

6.2. Sensitivity Results

In this section, we start with an analysis of the possible effect of 1 % dip angle along the X-axis on CO_2 plume. For this, we compare in Figure 7 the CO_2 plume at 10 days as obtained in each case (the reference case with Y5% and the case with two

dips angles Y5%- X1%). In the reference case, the plume is elliptical and centered on the injection Y-axis (i.e. the main flow direction), whereas in the other case, the plume spreads over the horizontal plan and advances in the side of the low altitude of aquifer top-surface (from the upper-right to the lower-left boundaries). We note also that the width of the spreading is more important in the case of two dips angles (almost equal to 7 m versus 4 m in the reference case) as the one along the X-axis comes to enhance the effect of the transverse dispersion. Thus, 1 % dip angle along the X-axis changes significantly the plume shape as it is advected with the flow. Note that in this case, the third observation well becomes useless since the plume passes on the other side and in such a case we risk to observe nothing in this well. Or, if the dip angle was in the opposite direction, this third well becomes very important for the measurements. For this reason particular importance should be given to the well placement with regard to the value of this parameter which has to be estimated as the drilling progresses.

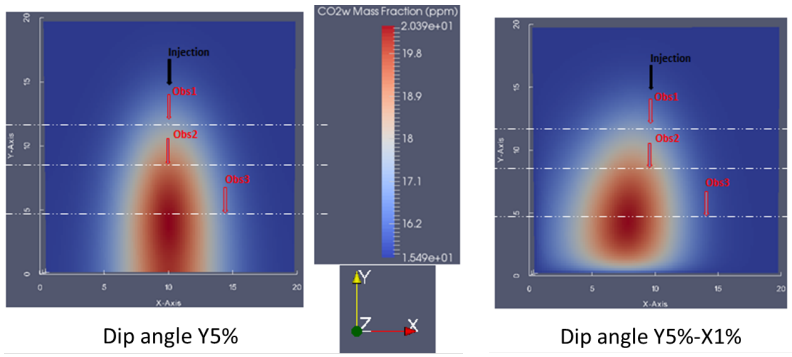

(a) (b)

Figure 7: Zoom-in (top view) at the effect of 1 % dip angle along X-axis on the dissolved CO_2 plume comparing to the reference case at $t = 10$ days: (a) reference case with Y5% and (b) top aquifer with two dips angles Y5%- X1%.

The effect of the dip angle on the evolution of CO_2 concentration can be quantitatively evaluated via Figure 8. It shows the variation of the CO_2 mass fraction with time at the three observation wells according to each simulation case. As expected, the impact of the dip angle is clearer and more significant on the measurements in the

third well, while in the other wells, the results are very similar to those obtained in the reference case. To finish with the effect of the aquifer characteristics, we consider the second parameter which is the water table level. Figure 8 shows that the model simulations are very sensitive to this parameter in virtually the three wells since the maximum values are reached in this case. Regarding the other parameters, dispersivity appears to be the parameter that has the most impact on CO_2 migration compared to permeability and especially when the longitudinal dispersivity is set at very low values (as given by the case $\alpha_L = 0.3$ m).

Let us now consider the sensitivity results: in the first well, the maximum value that can be measured is 51 ppm in the case of lowest water table or when $\alpha_L = 0.3$ m, and a minimum value of 28 ppm can be obtained in the case of $k = 10$ D or $\alpha_L = 3$ m. However, the time of reaching these maximum values does not vary too much and it ranges over 1-3 days. Almost the same dependence can be noticed in the second well as the maximum value varies from 21 to 35 ppm and the time necessary for reaching it is after 3 to 5 days from the injection. For the third well, we found that the lowest water table has a significant impact on the temporal evolution of the CO_2 concentration; in this case, the maximum value is 19.5 ppm and it is reached after 9-10 days. This indicates a large spreading of the CO_2 plume in the transverse main direction of the water flow, as it will be confirmed hereinafter. This expected result is explained by the decrease of the transversal dispersivity flux along the vertical axis induced by the decrease of the aquifer thickness in case of low water table.

Figure 9 shows the variation of the CO_2 mass fraction across the sections XZ of the observation wells. These profiles are presented at the times ensuring the maximum concentration in each simulation case.

The spreading of the CO_2 concentrations is still clear in all cases and takes the form of Gaussian curve, but with varying widths at half maximum that range over 3-4 m in Obs1, 4-6 m in Obs2, and 4-12 m in Obs3. The maximum width is always obtained in case of simulation with lowest water table level. The dependence of the main model predictions on CO_2 concentration, that are the maximum CO_2 mass fraction that can be measured in each well ($w_{\max}$), the time of reaching this peak ($t_{\max}$) and the full width at half maximum of the Gaussian spreading (L_c), are summarized in Table 3. The method

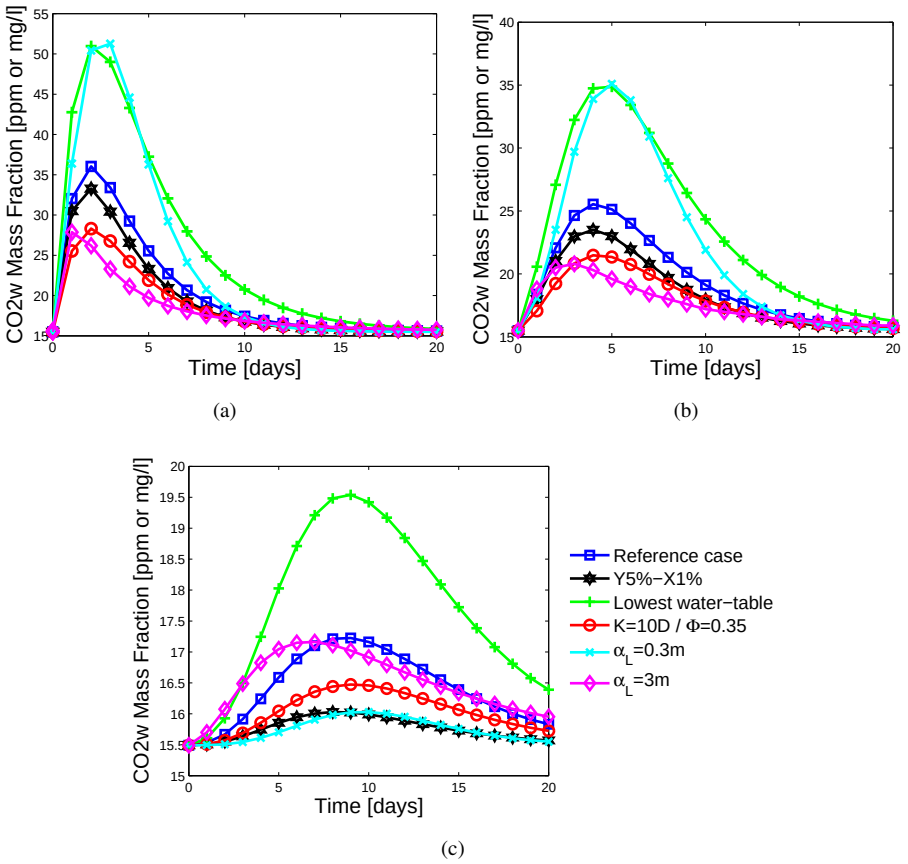

Figure 8: Evolution of the mass fraction of CO_2 versus time at the three observation wells: (a) at Obs1, (b) at Obs2 and (c) at Obs3. Note that the "reference" case corresponds to the simulation with $k = 6$ D, $\phi = 0.2$, highest water table, $\alpha_L = 1$ m and single dip angle of 5 % along the Y-axis.

to calculate the full width at half maximum (L_c) is outlined in Figure 10. Note that the latter summary table is very useful in the field at the time of the experiment since it provides the times at which sampling and measurements can be performed without losing any precision and gives insights into CO_2 plume position and velocity at which it advances. The table also checks that in all the studied cases, CO2 and tracers can be detected by the measuring equipment since CO2 concentration is greater than ppm scale and krypton concentration is greater than ppb scale.

As a conclusion of this study, we advice to proceed with the following steps for

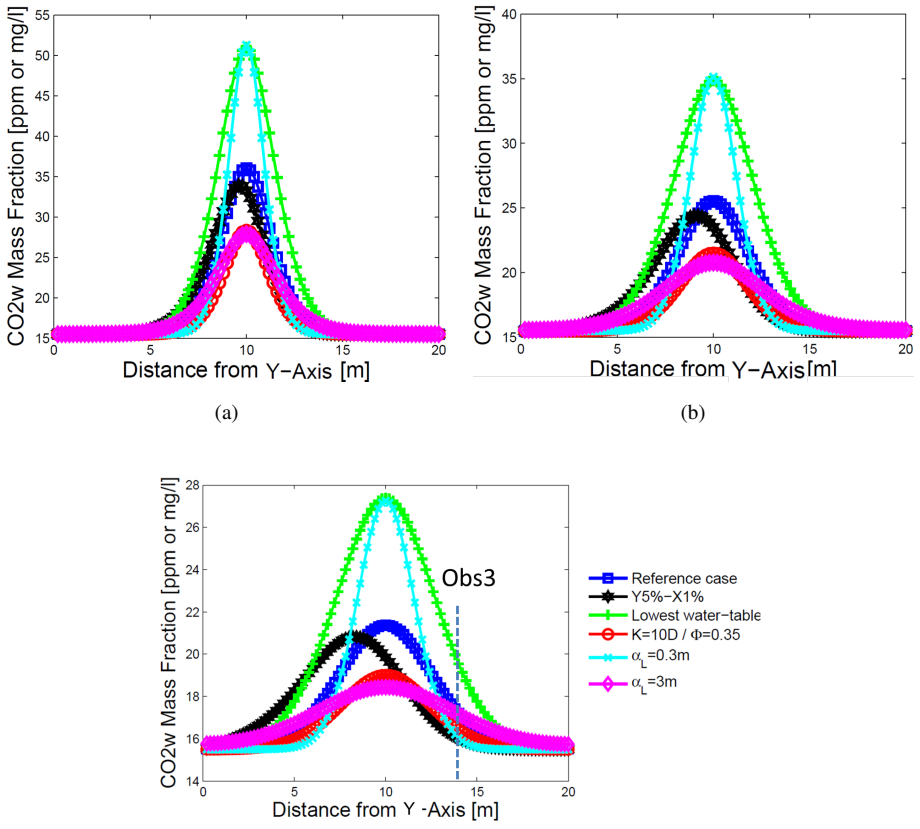

Figure 9: Variations of the mass fraction of CO_2 in the sections XZ of the observation wells (at the time ensuring the maximum of CO_2 concentrations for each parameter, cf. Figure 8): (a) Obs1, (b) Obs2 and (c) Obs3.

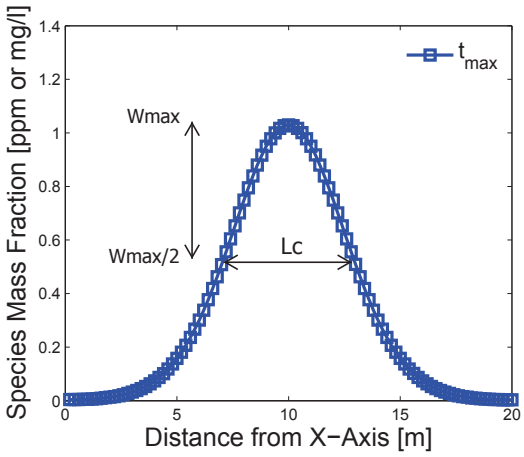

Figure 10: Method to calculate the full width at half maximum (L_c).

placing the observation wells in the Saint-Emilion experimental site. During the well drilling phase, we should start by drilling three wells forming a rectangular triangle to measure the water table level at each well. The estimation of the dip angle along the X and Y-axis from these measurements will define the main direction of the aquifer flow. Then, other wells will be drilled to perform additional measurements to accurately monitor the CO_2 plume. They will be placed to cover a zone as a diamond-shape oriented in the main flow direction to optimize the site monitoring. Indeed, the species migrate both by advection and longitudinal and transversal dispersion. The diamond dimensions will be defined from the simulated species concentration taking into account the parameter uncertainty. Thus, a new fluid flow simulation using the measured data of the water table level and of the two dip angles should be performed to reduce the uncertainty of the diamond size.

Table 3: Summary of the sensitivity results of CO_2 and krypton migration to the uncertain parameters. The "reference" case refers to to the simulation conducted with $k = 6$ D, $\phi = 0.2$, highest water table, $\alpha_L = 1$ m and single dip angle of 5 % along the Y-axis.

	Reference case			$k = 10$ D - $\phi = 0.35$			Y5% - X1%			Lowest water table			$\alpha_L = 0.3$ m			$\alpha_L = 3$ m		
	t_{max} (days)	w_{max} (ppm)	L_c (m)	t_{max} (days)	w_{max} (ppm)	L_c (m)	t_{max} (days)	w_{max} (ppm)	L_c (m)	t_{max} (days)	w_{max} (ppm)	L_c (m)	t_{max} (days)	w_{max} (ppm)	L_c (m)	t_{max} (days)	w_{max} (ppm)	L_c (m)
For CO_2 concentration																		
Obs1	2	37	3.5	2	28	3.5	2	33	4	2	51	4	3	51	3	1	28	4
Obs2	4	26	4.5	4	22	4	4	24	6	5	35	6	5	35	4	3	21	6
Obs3	8	17	6	8	16.5	6	7	16	7	9	19.5	6.5	9	16	4	6	17	12
For krypton concentration																		
Obs1	-	3.5	-	-	2.2	-	-	3.2	-	-	6.2	-	-	6.2	-	-	2.2	-
Obs2	-	1.7	-	-	1	-	-	1.5	-	-	3.5	-	-	3.5	-	-	1	-
Obs3	-	0.3	-	-	0.2	-	-	0.1	-	-	0.7	-	-	0.1	-	-	0.3	-

7. Conclusions

The aim of this work was sizing both in time and space the planned experiment that consists in injecting dissolved CO_2 and tracer gases in water in the saturated zone of the Saint-Emilion experimental site. This objective was met by first determining the injection flow rate and the injected volume considering the site constraints. Thus, 200 l of solution containing the studied dissolved species was assumed to be injected at a volume rate of 2,520 ml/min. Then, the analysis of the simulation results allowed us to determine the size plume evolution with time, the date when the maximum of each species concentration is reached for three observation wells and the return time to the initial state of the system. The CO_2 plume size analysis showed that the average full width at half maximum is 3.5 m at the first observation well and 4.5 m at the second one, two days later due to transversal dispersion. We also observed that the maximum of CO_2 concentration is reached at about 2 days at 3 m and 4 days at 6 m from the injection well with a return at the initial state after 20 days.

Then, the sensitivity analysis of this work leads us to quantify the effect of the uncertain model parameters on the size plume and the date when the maximum of each species concentration is reached as well as to identify the sensitive parameters which have the strongest influence on the model predictions. The studied uncertain parameters were the dip angle along the X-axis, the longitudinal and transversal dispersivity, the water table level and the permeability and porosity parameters. The study concluded that the most sensitive parameters of this model are the dispersivity and the water table level. The permeability and porosity parameters and the dip angle along the X-axis have less effects. However, this study showed that this dip angle is a very important data that is necessary to measure to avoid drilling useless observation wells.

Finally, the results of this work come to verify that the proposed locations for injection and observation wells allow us to provide sufficient coverage of the measurements while considering the technical constraints for drilling on site and under some simplifying assumptions that have been studied and evaluated in this work. We also advice to start the well drilling phase by the measurement of the water table level at the three first wells and by the estimation of the dip angle along the X and Y-axis from these

measures since these parameters are important for this site to know respectively the area dimensions for monitoring and the fluid flow direction. Other wells will be drilled to perform additional measurements to accurately monitor the CO_2 plume. They will be placed to cover a zone as a diamond-shape to optimize the site monitoring. The final position of these wells will be specified in the next papers. In total, eight wells are planned to be built for this site.

This study constitutes the first step in the modeling work of the Aquifer-CO_2Leak project. Several points will be addressed within the future works after the injection experiment such as (1) the reactive transport modeling to consider the fluid rock interactions that occurs in carbonates of Saint Emilion, (2) the calibration of the fluid flow model by adjusting the uncertain parameters that was discussed herein and the calibration of the geochemical model and (3) the interpretation of the experimental measurements.

The simulation work presented in this article and the scheduling of the future one after the experiment in Saint-Emilion show that simulation is essential at different steps of a project life whether it is a small-scale pilot as Saint-Emilion or a CO_2 storage at large scale. Simulation is necessary (1) to design the site for both the injection process (well position, rate, ...) and the monitoring network (observation wells, soil sensors to detect surface movement or gas leakage, ...) and (2) to predict the CO_2 plume migration and its impacts. At each step, the model is more complicated by integrating static and dynamic information measured in-situ and the uncertainties of the simulation results are reduced.

Acknowledgments

This research work was conducted within the Aquifer-CO_2Leak project which is funded by the ADEME and the Région Nouvelle Aquitaine from France. The authors are grateful to IFPEN and research unit EA 4592 G&E ENSEGID-Bordeaux-INP for permission to publish this work and also all the partners of this project for useful discussions.

References

[1] GISTEMP-Team, Giss Surface Temperature Analysis (GISTEMP), NASA Goddard Institute for Space Studies (2018) Dataset accessed 2018–10–30.
URL https://data.giss.nasa.gov/gistemp/

[2] J. Hansen, R. Ruedy, M. Sato, K. Lo, Global surface temperature change, Rev. Geophys. 48 (2010) RG4004.

[3] GISTEMP-Team, Climate change: How do we know?, NASA Global Climate Change (2018) Dataset accessed 2018–10–30.
URL https://climate.nasa.gov/evidence/

[4] Total, Carbon capture and storage: the Lacq pilot. Project and injection period 2006-2013, Global CCS Institute (2015) 274.

[5] J. Monne, The Lacq CCS Pilot, a First, International Conference on Health, Safety and Environment in Oil and Gas Exploration and Production 13 (2012) SPE–157157–MS. doi:10.2118/157157-MS.

[6] P. Singh, M. Haines, A Review of Existing Carbon Capture and Storage Cluster Projects and Future Opportunities, Energy Procedia 63 (2014) 7247 – 7260. doi:https://doi.org/10.1016/j.egypro.2014.11.761.

[7] Z. Kapetaki, J. Simjanovic, J. Hetland, European Carbon Capture and Storage Project Network: Overview of the Status and Developments, Energy Procedia 86 (2016) 12 – 21. doi:https://doi.org/10.1016/j.egypro.2016.01.002.

[8] R. Nataly, T. X. Jun, Energy related CO_2 emissions and the progress on CCS projects: A review, Renewable and Sustainable Energy Reviews 31 (2014) 368 – 385. doi:https://doi.org/10.1016/j.rser.2013.12.002.

[9] Club-CO_2, Carbon Capture, Use and Storage (CCUS): a solution for the future (2011) Dataset accessed 2018–10–31.
URL http://www.captage-stockage-valorisation-co2.fr/en/deep-saline-aquifers

[10] C. Oldenburg, U. Andre, Coupled Vadose Zone and Atmospheric Surface-Layer Transport of Carbon Dioxide from Geologic Carbon Sequestration Sites, Vadose Zone Journal 3 (3) (2004) 848. doi:10.2113/3.3.848.

[11] C. White, B. Strazisar, E. Granite, J. Hoffman, H. Pennline, Separation and capture of CO_2 from large stationary sources and sequestration in geological formations coalbeds and deep saline aquifers, Journal of Air and Waste Management Association 53 (2003) 645–715.

[12] G. Cohen, C. Loisy, C. Laveuf, O. L. Roux, P. Delaplace, C. Magnier, V. Rouchon, B. Garcia, A. Cerepi, The CO_2-Vadose Project: Experimental study and modelling of CO_2 induced leakage and tracers associated in the carbonate vadose zone, International Journal of Greenhouse Gas Control 14 (2013) 128 – 140. doi:https://doi.org/10.1016/j.ijggc.2013.01.008.

[13] F. Gal, K. Michel, Z. Pokryszka, S. Lafortune, B. Garcia, V. Rouchon, P. de Donato, J. Pironon, O. Barres, N. Taquet, G. Radilla, C. Prinet, J. Hy-Billiot, M. Lescanne, P. Cellier, H. Lucas, F. Gibert, Study of the environmental variability of gaseous emanations over a CO_2 injection pilot: Application to the French Pyrenean foreland, International Journal of Greenhouse Gas Control 21 (2014) 177 – 190. doi:https://doi.org/10.1016/j.ijggc.2013.12.015.

[14] O. L. Roux, G. Cohen, C. Loisy, C. Laveuf, P. Delaplace, C. Magnier, V. Rouchon, A. Cerepi, B. Garcia, The CO_2-Vadose Project: Time-lapse geoelectrical monitoring during CO_2 diffusion in the carbonate vadose zone, International Journal of Greenhouse Gas Control 16 (2013) 156 – 166. doi:https://doi.org/10.1016/j.ijggc.2013.03.016.

[15] K. Gilles, M. Gilles, Monitoring pour le stockage du CO_2 et la production des hydrocarbures, Oil Gas Sci. Technol. - Rev. IFP Energies nouvelles 67 (2) (2012) 187–192. doi:10.2516/ogst/2011178.
URL https://doi.org/10.2516/ogst/2011178

[16] C. Loisy, G. Cohen, C. Laveuf, O. L. Roux, P. Delaplace, C. Magnier, V. Rouchon, A. Cerepi, B. Garcia, The CO_2-Vadose Project: Dynamics of the natural CO_2 in

a carbonate vadose zone, International Journal of Greenhouse Gas Control 14 (2013) 97 – 112. doi:https://doi.org/10.1016/j.ijggc.2012.12.017.

[17] B. Garcia, P. Delaplace, V. Rouchon, C. Magnier, C. Loisy, G. Cohen, C. Laveuf, O. L. Roux, A. Cerepi, The CO_2-Vadose Project: Numerical modeling to perform a geochemical monitoring methodology and baseline performance assessment for various geochemical variables (gas flux, gas composition, stable isotopes and noble gases) in the carbonate vadose zone, International Journal of Greenhouse Gas Control 14 (2013) 247 – 258. doi:https://doi.org/10.1016/j.ijggc.2013.01.029.

[18] S. Beaubien, D. Jones, F. Gal, A. Barkwith, G. Braibant, J.-C. Baubron, G. Ciotoli, S. Graziani, T. Lister, S. Lombardi, K. Michel, F. Quattrocchi, M. Strutt, Monitoring of near-surface gas geochemistry at the Weyburn, Canada, CO_2-EOR site 2001-2011, International Journal of Greenhouse Gas Control 16 (2013) S236–S262.

[19] M. Myers, L. Stalker, B. Pejcic, A. Ross, Tracers-past, present and future applications in CO_2 geosequestration, Appl. Geochem. 30 (2013) 125–135.

[20] C. Oldenburg, A. Unger, Coupled subsurface-surface layer gas transport and dispersion for geologic carbon sequestration seepage simulation, Tagungsbeitrag, TOUGH Symposium, 12-14.

[21] J. Lewicki, C. Oldenburg, L. Dobeck, L. Spangler, Surface CO_2 leakage during two shallow subsurface CO_2 releases, Geophys. Res. Lett. 34.

[22] S. Schlomer, I. Moller, M. Furche, Baseline soil gas measurements as part of a monitoring concept above a projected CO_2 injection formation. A case study from Northern, International Journal of Greenhouse Gas Control 20 (2014) 57–72.

[23] G. Barron-Gafford, R. Scott, G. Jenerette, T. Huxman, The relative controls of temperature, soil moisture and plant functional group on soil CO_2 efflux at diel seasonal and annual scales, J. Geophys. Res. 116 (G01023).

[24] Y. Le Gallo, L. Trenty, A. Michel, S. Vidal-Gilbert, T. Parra, L. Jeannin, Long-term flow simulation of CO_2 storage in saline aquifers, Proceedings of the 8th International Conference on Greenhouse Gas Control Technologies, 19-23 June, Trondheim, Norway.

[25] A. Estublier, P. Bachaud, A. Michel, N. Maurand, J.-P. Deflandre, Long-term fate of CO_2 in a saline aquifer: modeling issues, Energy Procedia 63 (2014) 3464–3474.

[26] A. Estublier, A. Fornel, E. Brosse, P. Houel, J.-C. Lecomte, J. Delmas, O. Vincke, Simulation of a Potential CO_2 Storage in the West Paris Basin: Site Characterization and Assessment of the Long-Term Hydrodynamical and Geochemical Impacts Induced by the CO_2 Injection, Oil and Gas Science and Technology Rev. IFP Energies nouvelles 72 (22).

[27] H. Class, A benchmark study on problems related to CO_2 storage in geologic formations : Summary and discussion of the results - original paper, Computational Geosciences 13 (4) (2009) 409–434.

[28] J.-M. Nordbotten, Uncertainties in practical simulation of CO_2 storage, International Journal of Greenhouse Gas Control 9 (0) (2012) 234–242.

[29] A. Fick, On liquid diffusion, Journal of Membrane Science 100 (1) (1995) 33 – 38. doi:https://doi.org/10.1016/0376-7388(94)00230-V.

[30] L. W. Gelhar, C. Welty, K. R. Rehfeldt, A critical review of data on field-scale dispersion in aquifers, Water Resources Research 28 (1992) 1955–1974. doi:10.1029/92WR00607.